

Self-constructing a lattice-oxygen-stabilized interface in Li-rich cathodes to enable high-energy all-solid-state batteries

Xiangqun Xu, Shiyong Chu, Sheng Xu, Shaohua Guo*, Haoshen Zhou*

X.Q. Xu, S.Y. Chu, S. Xu, S.H. Guo, H.S. Zhou

College of Engineering and Applied Sciences, Jiangsu Key Laboratory of Artificial Functional Materials, National Laboratory of Solid State Microstructures, Collaborative Innovation Center of Advanced Microstructures, and Frontiers Science Center for Critical Earth Material Cycling, Nanjing University, Nanjing, 210023, China.

E-mail: shguo@nju.edu.cn (S.H. Guo); hszhou@nju.edu.cn (H.S. Zhou)

X.Q. Xu, S.Y. Chu, S. Xu, S.H. Guo

Lab of Power and Energy Storage Batteries, Shenzhen Research Institute of Nanjing University, Shenzhen, 518057 China

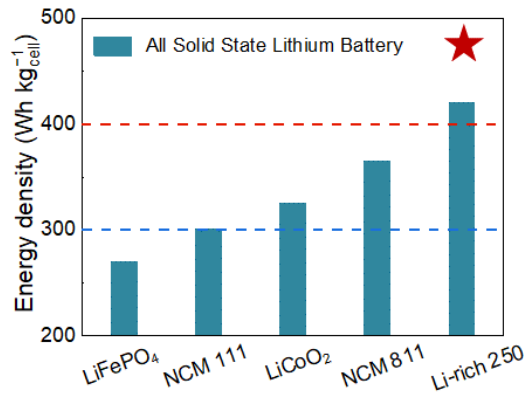


Figure S1 Energy density of ASSLBs with various typical cathode materials.

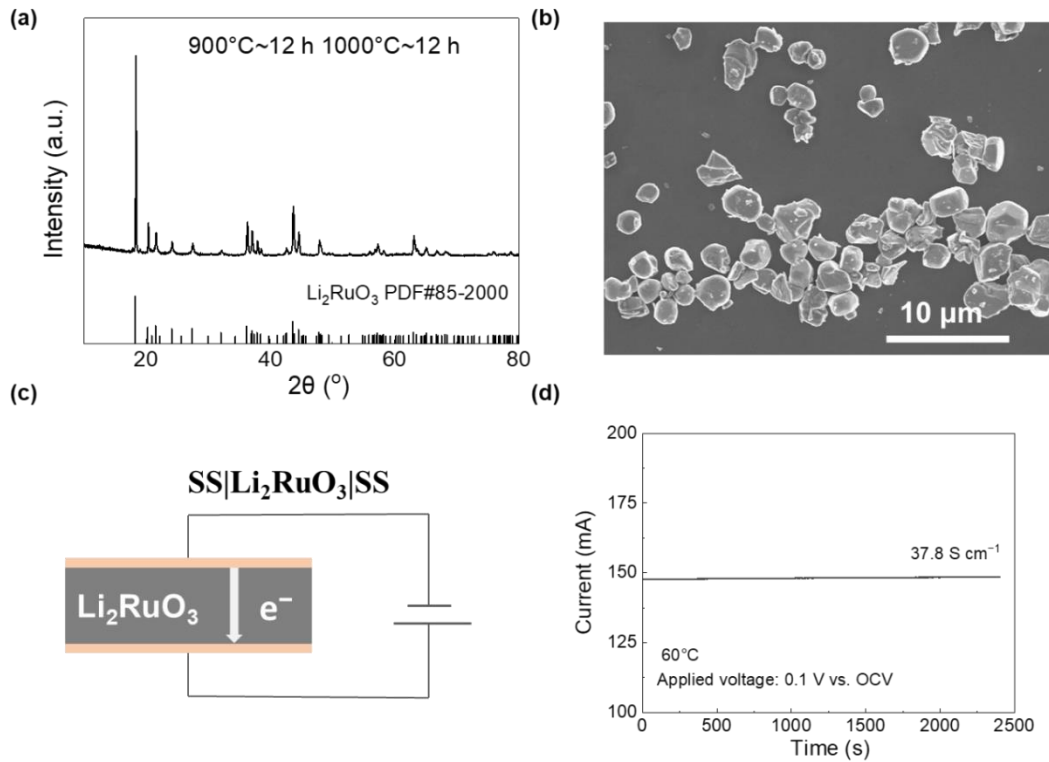


Figure S2 (a) XRD pattern. (b) SEM image of LRO powders. (c) Schematic diagram and (d) the curve for DC polarization test of a symmetric cell (stainless steels | LRO | stainless steels) at 60°C .

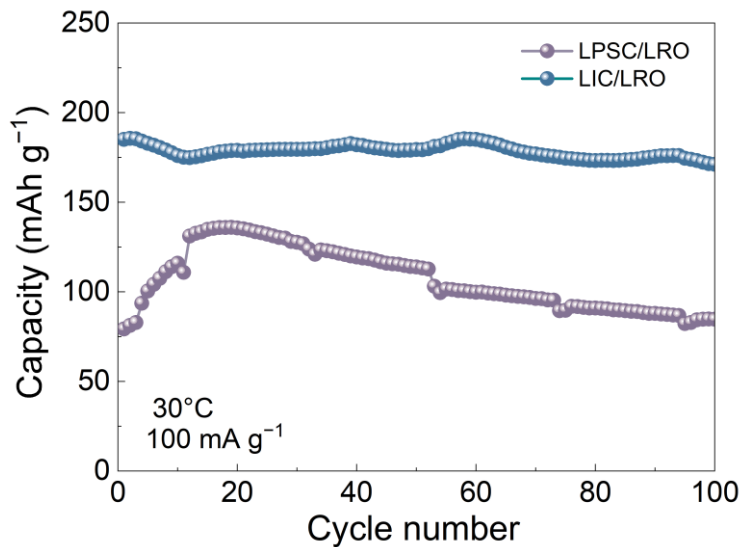


Figure S3 Cycling stability of LIC/LRO and LPSC/LRO in ASSLBs at 100 mA g⁻¹ under 30°C.

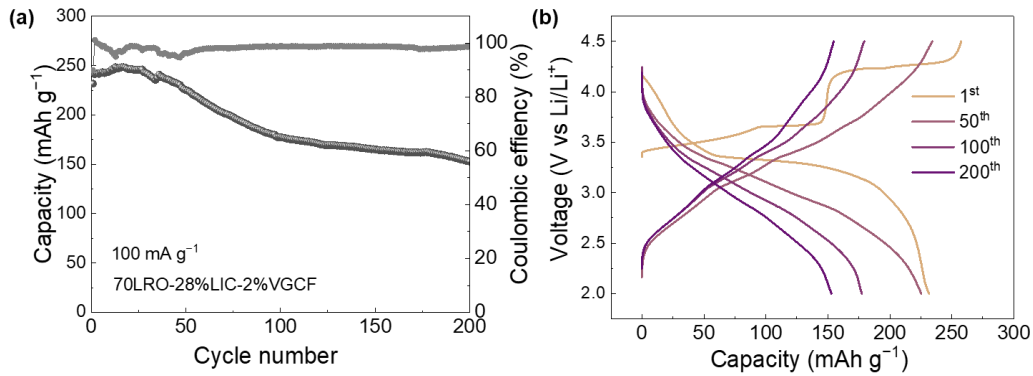


Figure S4 Cycling stability curves of LIC/LRO with 2wt% VGCF at 100 mA g^{-1} at 60°C .

The composite cathode with conductive carbon shows a capacity retention of only 65.9% after 200 cycles.

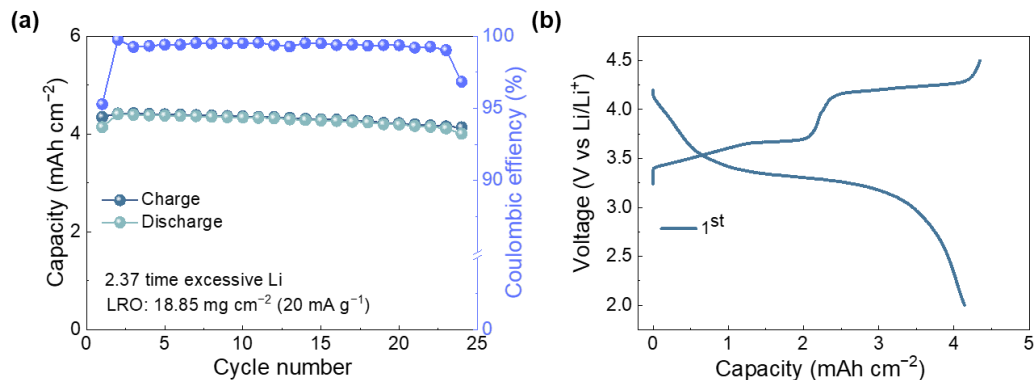


Figure S5 (a) Cycling stability of LIC/LRO with a high loading. (b) Corresponding charge–discharge profiles.

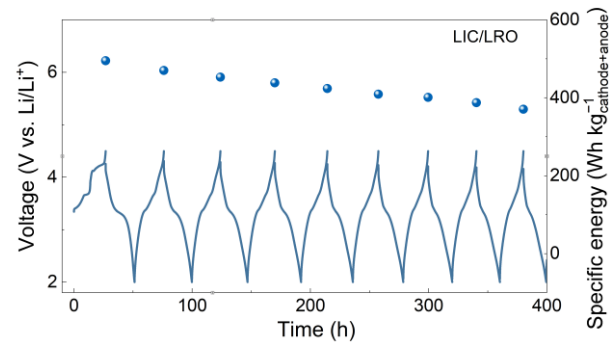


Figure S6 Specific energy and corresponding discharge-charge curves of LIC/LRO ASSB at 20 mA g⁻¹ (30wt%-LIC/70wt%-LRO cathode 4.9 mg, Li anode 0.5 mg).

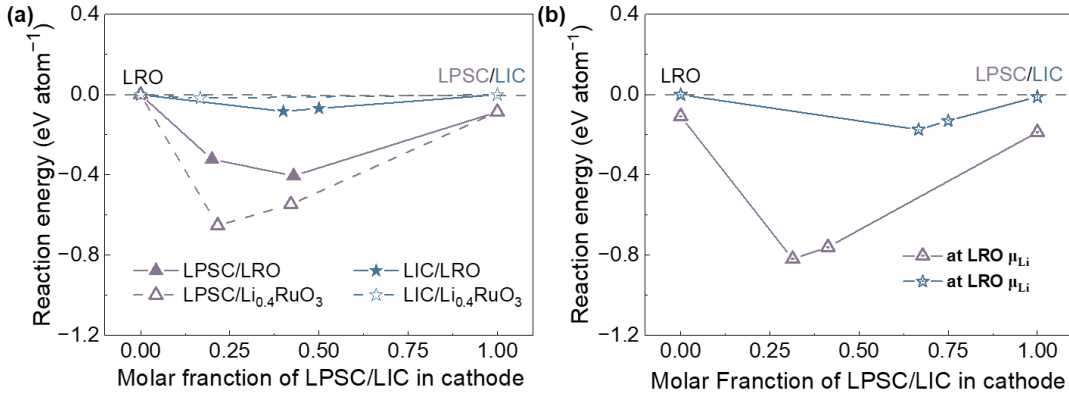


Figure S7 (a) The mutual reaction energy of LIC and LPSC with pristine and charged LRO. (b) The mutual reaction energy of LIC and LPSC with LRO at Li chemical potential μ_{Li} .

The calculation results show that the LPSC/LRO interface is thermodynamically unstable and suffers spontaneous chemical decomposition reactions with a reaction energy of $-0.404 \text{ eV atom}^{-1}$. In addition, the reaction energy of LPSC/Li_{0.4}RuO₃ (delithiated cathode) changes to $-0.652 \text{ eV atom}^{-1}$, indicating that the interface is more unstable at 4.5 V. The interface stability can be significantly improved when LIC replaces LPSC in the composite cathodes. In this case, the reaction energy of LIC/LRO is $-0.083 \text{ eV atom}^{-1}$ (almost no reaction). Under the full charge state, the reaction energy is only $-0.017 \text{ eV atom}^{-1}$, meaning a stable interface. In addition, at Li chemical potential μ_{Li} , LIC/LRO also shows a more stable interface than LPSC/LRO

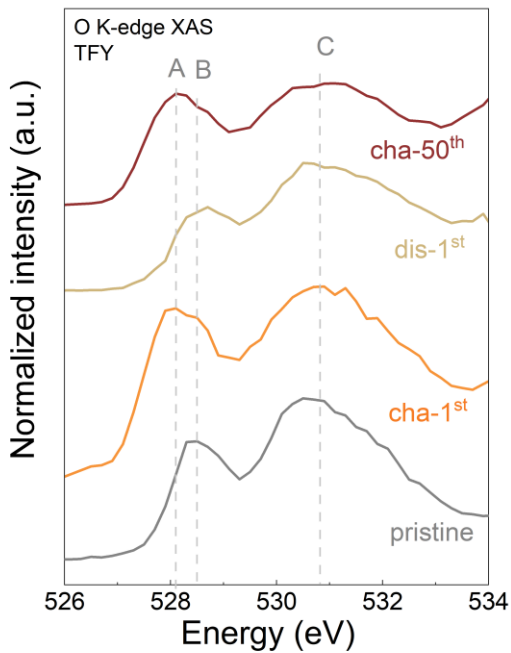


Figure S8 O K-edge XAS spectra of LIC/LRO under different states. Two peaks, B and C, representing to the TM 3d/4d-O 2p t_{2g} and e_g hybridized states, appear in the spectra at 528.5 and 530.9 eV, respectively ¹. In the fully charged state (4.5 V) of LIC/LRO, the intensity of peak B increases and a new peak A at 528.1 eV appears, suggesting the remove of electron from the lattice oxygen or the lattice oxygen is oxidized during charging ², which is in agreement with the O 1s XPS spectra in Figure 3b. Even after 50 cycles, LIC/LRO still shows the oxidization of lattice oxygen. When LIC/LRO is discharged to 2.0 V, the intensity of peak B decreases and the peak A disappears, indicating the oxidized lattice oxygen ($O^{(2-n)-}$) is reversibly reduced to O^{2-} .

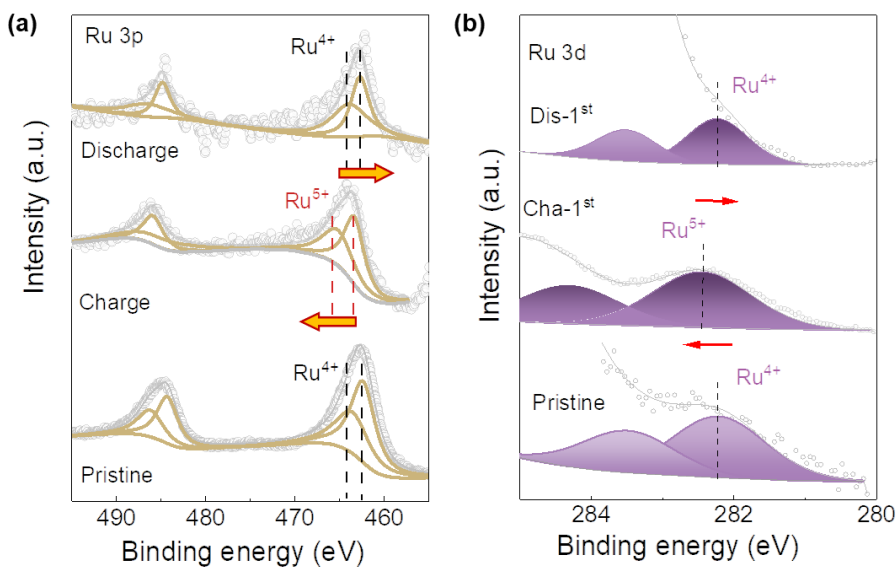


Figure S9 (a) Ru 3p and (b) Ru 3d XPS spectra for LIC/LRO under different states. The valence state change of the cation Ru was also detected by XPS. The Ru 3p peaks are shifted towards the high binding energy during charging, suggesting the oxidation of Ru⁴⁺ to Ru⁵⁺³. Upon discharge, the peak positions revert to their initial positions, indicating the reduction of Ru⁵⁺ to Ru⁴⁺. The reversible redox of Ru is further demonstrated by the corresponding changes of Ru 3d correlation spectra ⁴.

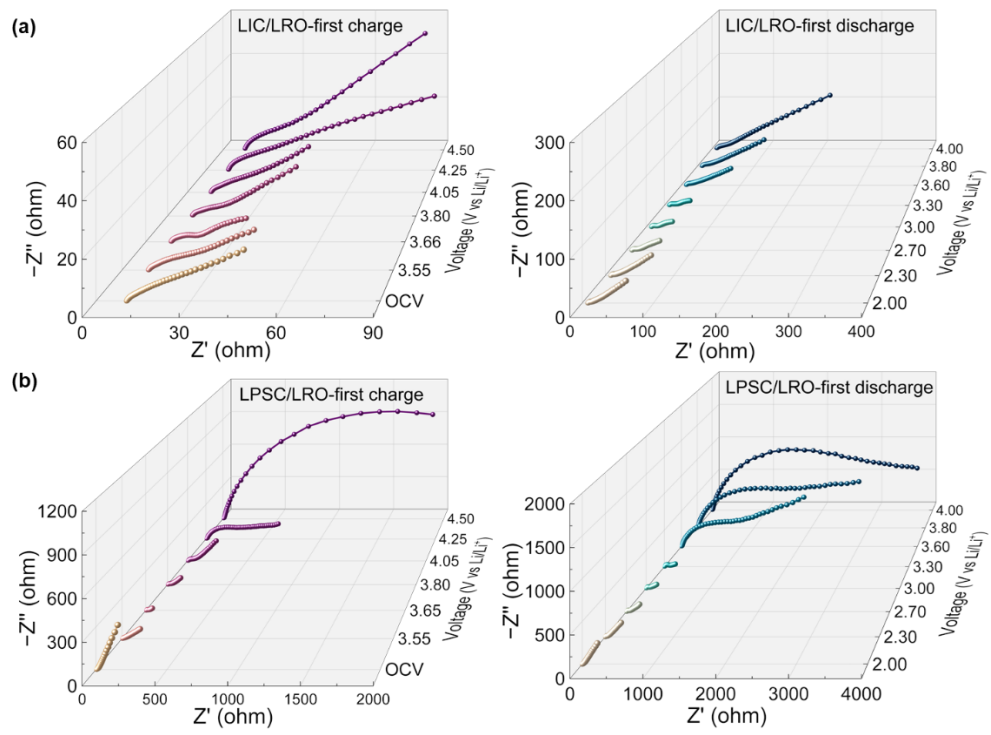


Figure S10 Nyquist plots for (a) LIC/LRO and (b) LPSC/LRO during the first discharge process.

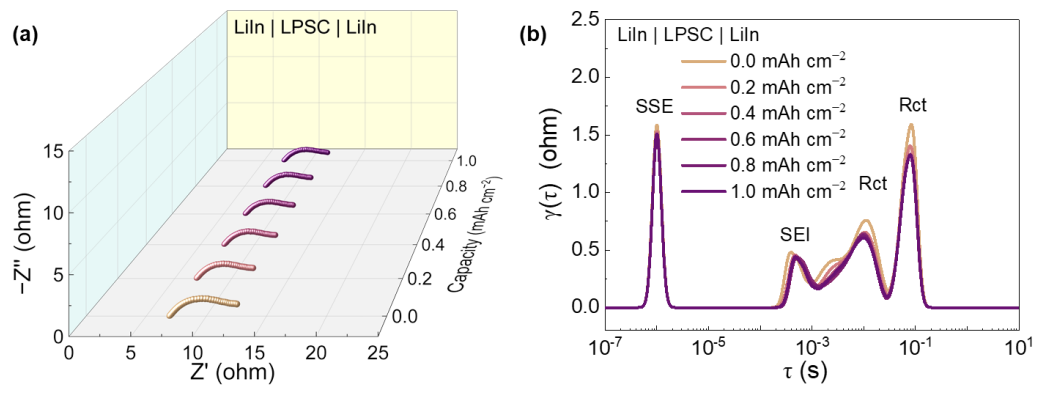


Figure S11 (a) Interfacial impedance evolution of the $\text{LiIn} \mid \text{LPSC} \mid \text{LiIn}$ symmetrical cell charged at about 1 mAh cm^{-2} . (b) The DRT profiles transformation of EIS.

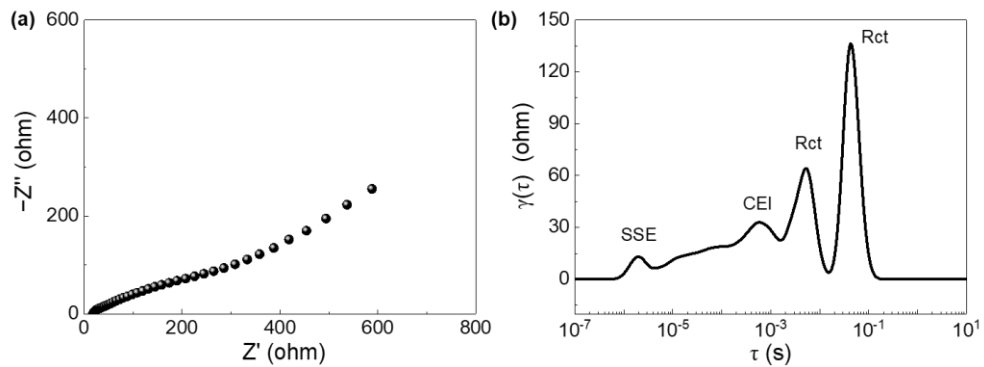


Figure S12 (a) Interfacial impedance of the LIC/LRO (charge) | LIC/LRO (pristine) cell and corresponding (b) DRT profiles transformation of EIS.

Table S1. First-cycle discharge capacity, current density, voltage range, and energy density of the ASSLBs.

Ref.	Cathode@coating	Voltage range	Current density (mA g ⁻¹)	Discharge capacity (mAh g ⁻¹)	Energy density (Wh kg ⁻¹)
5	Bare/LiFePO ₄	2.0-4.2	13	145	494.45
6	Bare/LiFePO ₄	2.5-3.9	0.1C	148.8	501.72
7	NCM90@Al	2.7-4.3	40	156.8	595.84
8	NCM811@LPO	2.7-4.5	0.2C	170.6	632.926
9	SC-NCM83	2.5-4.4	20	175.5	668.655
10	NCM8@LNO/LCO	2.7-4.38	20	182.4	687.648
11	NCM811@LNO	2.8-4.2	32	189	697.41
12	NCM811@LSO	2.4-4.2	10	188	705
13	NCM75	3.0-4.3	15	194	737.2
14	PC-NCA811	3.0-4.3	20	164	626.48
15	NCA@LNO	2.8-4.2	13	177.3	661.329
16	NCA@LNO	2.72-4.32	12	184.1	688.534
17	SC-NCA811	2.85-4.35	18	187	712.47
14	PC-NCA811	3.0-4.3	20	191	731.53
14	SC-NCA811	3.0-4.3	20	191	731.53
14	SC-NCA811	3.0-4.3	20	201	769.83
18	LCO@LZP	2.6-4.5	28	143.3	543.107
19	LCO@LBBO	2.6-4.3	0.1C	153.8	598.282
20	LCO@LTO/LBO	2.6-4.5	36	170.2	667.184
21	LCO@LNTO	2.6-4.5		176	693
22	LMCN	2.0-4.8	20	196	701.68
23	LRO	2.0-4.3	10	220	721.6
This work	LRO	2.0-4.5	20	294	970

Table S2. Phase equilibria and decomposition energies of the LPSC/LRO and LIC/LCO interfaces. x is the molar fraction of LPSC/LIC in [x·LPSC/LIC + (1-x) LRO].

Celectrode	State	x	Phase equilibria	ΔH_D (eV atom ⁻¹)
Chemical reaction				
LPSC/LRO	Full-lithiated	0.2	Li ₂ SO ₄ Li ₃ PO ₄ Li ₂ S LiCl	-0.322
		0.429	Li ₃ PO ₄ Li ₂ S RuS ₂ LiCl	-0.404
	De-lithiated	0.216	Li ₂ SO ₄ Li ₃ PO ₄ RuS ₂ LiCl	-0.652
		0.421	Li ₃ PO ₄ Li ₂ S RuS ₂ LiCl S ₈ O	-0.546
Electrochemical reaction				
LIC/LRO	At LRO μLi	0.314	Li ₂ SO ₄ Li ₃ PO ₄ RuS ₂ LiCl	-0.819
		0.413	S ₈ O Li ₃ PO ₄ RuS ₂ LiCl	-0.759
Chemical reaction				
LIC/LRO	Full-lithiated	0.4	In ₂ O ₃ RuO ₂ LiCl	-0.083
		0.5	RuO ₂ InClO LiCl	-0.068
	De-lithiated	0.167	InClO LiCl RuO ₄ RuO ₂	-0.017
Electrochemical reaction				
LIC/LRO	At LRO μLi	0.314	Li ₂ SO ₄ Li ₃ PO ₄ RuS ₂ LiCl	-0.819
		0.413	S ₈ O Li ₃ PO ₄ RuS ₂ LiCl	-0.759

SI References

1. N. Voronina, N. Yaqoob, H. J. Kim, K. S. Lee, H. D. Lim, H. G. Jung, O. Guillon, P. Kaghazchi and S. T. Myung, *Adv. Energy Mater.*, 2021, **11**, 2100901.
2. B. Li, K. Kumar, I. Roy, A. V. Morozov, O. V. Emelyanova, L. Zhang, T. Koc, S. Belin, J. Cabana, R. Dedryvere, A. M. Abakumov and J. M. Tarascon, *Nat. Mater.*, 2022, **21**, 1165-1174.
3. Y. Qiao, S. Guo, K. Zhu, P. Liu, X. Li, K. Jiang, C.-J. Sun, M. Chen and H. Zhou, *Energy Environ. Sci.*, 2018, **11**, 299-305.
4. M. Sathiya, A. M. Abakumov, D. Foix, G. Rousse, K. Ramesha, M. Saubanere, M. L. Doublet, H. Vezin, C. P. Laisa, A. S. Prakash, D. Gonbeau, G. VanTendeloo and J. M. Tarascon, *Nat. Mater.*, 2015, **14**, 230-238.
5. T. Kim, K. Kim, S. Lee, G. Song, M. S. Jung and K. T. Lee, *Chem. Mater.*, 2022, **34**, 9159-9171.
6. Z. Deng, Z. Jin, D. C. Chen, D. X. Ni, M. Y. Tian, Y. J. Zhan, S. Li, Y. Sun, X. J. Huang and Y. S. Zhao, *ACS Appl. Mater. Interfaces*, 2022, **14**, 48619-48626.
7. X. Li, Y. Sun, Z. Wang, X. Wang, H. Zhang, D. Song, L. Zhang and L. Zhu, *Electrochim. Acta*, 2021, **391**, 138917.
8. S. X. Deng, X. Li, Z. H. Ren, W. H. Li, J. Luo, J. W. Liang, J. N. Liang, M. N. Banis, M. S. Li, Y. Zhao, X. N. Li, C. H. Wang, Y. P. Sun, Q. Sun, R. Y. Li, Y. F. Hu, H. Huang, L. Zhang, S. G. Lu, J. Luo and X. L. Sun, *Energy Storage Mater.*, 2020, **27**, 117-123.
9. W. Jiang, X. M. Fan, X. X. Zhu, Z. Z. Wu, Z. H. Li, R. Z. Huang, S. Zhao, X. M. Zeng, G. R. Hu, B. Zhang, S. Q. Zhang, L. Y. Zhu, L. J. Yan, M. Ling, L. G. Wang and C. D. Liang, *J. Power Sources*, 2021, **508**, 230335.
10. X. L. Li, Q. F. Sun, Z. Y. Wang, D. W. Song, H. Z. Zhang, X. X. Shi, C. L. Li, L. Q. Zhang and L. Y. Zhu, *J. Power Sources*, 2020, **456**, 227997.
11. S. J. Liu, L. Zhou, J. Han, K. H. Wen, S. D. Guan, C. J. Xue, Z. Zhang, B. Xu, Y. H. Lin, Y. Shen, L. L. Li and C. W. Nan, *Adv. Energy Mater.*, 2022, **12**, 2200660.
12. D. X. Cao, X. Sun, Y. J. Li, A. Anderson, W. Q. Lu and H. L. Zhu, *Adv. Mater.*, 2022, **34**, 24.
13. S. H. Jung, U. H. Kim, J. H. Kim, S. G. Jun, C. S. Yoon, Y. S. Jung and Y. K. Sun, *Adv. Energy Mater.*, 2020, **10**, 6.
14. Y. Han, S. H. Jung, H. Kwak, S. Jun, H. H. Kwak, J. H. Lee, S. T. Hong and Y. S. Jung, *Adv. Energy Mater.*, 2021, **11**, 2100126.
15. N. Ahmad, S. R. Sun, P. W. Yu and W. Yang, *Adv. Funct. Mater.*, 2022, **32**, 28.
16. X. L. Li, M. Liang, J. Sheng, D. W. Song, H. Z. Zhang, X. X. Shi and L. Q. Zhang, *Energy Storage Mater.*, 2019, **18**, 100-106.
17. X. S. Liu, B. Z. Zheng, J. Zhao, W. M. Zhao, Z. T. Liang, Y. Su, C. P. Xie, K. Zhou, Y. X. Xiang, J. P. Zhu, H. C. Wang, G. M. Zhong, Z. L. Gong, J. Y. Huang and Y. Yang, *Adv. Energy Mater.*, 2021, **11**, 8.
18. L. Wang, X. Sun, J. Ma, B. Chen, C. Li, J. Li, L. Chang, X. Yu, T. S. Chan, Z. Hu, M. Noked and G. Cui, *Adv. Energy Mater.*, 2021, **11**, 2100881.
19. C. W. Wang, S. J. Zhang, C. Lin, S. D. Xue, Y. P. Deng, B. K. Zhang, L. Y. Yang, X. Y. Yao, L. Y. Zeng, J. T. Li, F. Pan and Z. W. Yin, *Nano Energy*, 2023, **108**, 108192.
20. L. Feng, Z. W. Yin, C. W. Wang, Z. Li, S. J. Zhang, P. F. Zhang, Y. P. Deng, F. Pan, B. Zhang and Z. Lin, *Adv. Funct. Mater.*, 2023, **33**, 2210744.
21. W. He, N. Ahmad, S. Sun, X. Zhang, L. Ran, R. Shao, X. Wang and W. Yang, *Adv. Energy Mater.*, 2022, **13**, 2203703.
22. W. Du, Q. Shao, Y. Wei, C. Yan, P. Gao, Y. Lin, Y. Jiang, Y. Liu, X. Yu, M. Gao, W. Sun and H. Pan, *ACS Energy Lett.*, 2022, **7**, 3006-3014.
23. Y. Wu, K. Zhou, F. Ren, Y. Ha, Z. Liang, X. Zheng, Z. Wang, W. Yang, M. Zhang, M. Luo, C. Battaglia, W. Yang, L. Zhu, Z. Gong and Y. Yang, *Energy Environ. Sci.*, 2022, **15**, 3470-3482.